

Article

Combining APR-246 and HDAC-Inhibitors: A Novel Targeted Treatment Option for Neuroblastoma

Michael Müller^{1,2,3}, Lisa Rösch^{1,2,4}, Sara Najafi^{1,2,5}, Charlotte Gatzweiler^{1,2,3}, Johannes Ridinger^{1,2}, Xenia F. Gerloff^{1,2,5}, David T. W. Jones^{1,6}, Jochen Baßler⁷ , Sina Kreth^{1,8}, Sabine Stainczyk^{1,8} , Karen Frese⁹, Benjamin Meder^{9,10}, Frank Westermann^{1,8}, Till Milde^{1,2,5}, Heike Peterziel^{1,2}, Olaf Witt^{1,2,5} and Ina Oehme^{1,2,*} 

- ¹ Hopp Children's Cancer Center Heidelberg (KiTZ), 69120 Heidelberg, Germany; mic.mueller@kitz-heidelberg.de (M.M.); l.roesch@kitz-heidelberg.de (L.R.); s.najafi@kitz-heidelberg.de (S.N.); charlotte.gatzweiler@kitz-heidelberg.de (C.G.); j.ridinger@kitz-heidelberg.de (J.R.); xenia.gerloff@dkfz-heidelberg.de (X.F.G.); david.jones@kitz-heidelberg.de (D.T.W.J.); s.kreth@kitz-heidelberg.de (S.K.); s.stainczyk@kitz-heidelberg.de (S.S.); f.westermann@kitz-heidelberg.de (F.W.); t.milde@kitz-heidelberg.de (T.M.); h.peterziel@kitz-heidelberg.de (H.P.); o.witt@kitz-heidelberg.de (O.W.)
- ² Clinical Cooperation Unit Pediatric Oncology, German Cancer Consortium (DKTK), German Cancer Research Center (DKFZ), 69120 Heidelberg, Germany
- ³ Faculty of Medicine, Heidelberg University, 69120 Heidelberg, Germany
- ⁴ Faculty of Biosciences, Heidelberg University, 69120 Heidelberg, Germany
- ⁵ Department of Pediatric Oncology, Hematology and Immunology, University of Heidelberg Medical Center, 69120 Heidelberg, Germany
- ⁶ Pediatric Glioma Research Group, German Cancer Research Center (DKFZ) and German Consortium for Translational Cancer Research (DKTK), 69120 Heidelberg, Germany
- ⁷ Biochemistry Center, Heidelberg University, 69120 Heidelberg, Germany; jochen.bassler@bzh.uni-heidelberg.de
- ⁸ Neuroblastoma Genomics, German Cancer Research Center (DKFZ), 69120 Heidelberg, Germany
- ⁹ Institute for Cardiomyopathies Heidelberg, Heidelberg University, 69120 Heidelberg, Germany; karen.frese@med.uni-heidelberg.de (K.F.); Benjamin.Meder@med.uni-heidelberg.de (B.M.)
- ¹⁰ Genome Technology Center, Stanford University, Stanford, CA 94304, USA
- * Correspondence: i.oehme@kitz-heidelberg.de



Citation: Müller, M.; Rösch, L.; Najafi, S.; Gatzweiler, C.; Ridinger, J.; Gerloff, X.F.; Jones, D.T.W.; Baßler, J.; Kreth, S.; Stainczyk, S.; et al. Combining APR-246 and HDAC-Inhibitors: A Novel Targeted Treatment Option for Neuroblastoma. *Cancers* **2021**, *13*, 4476. <https://doi.org/10.3390/cancers13174476>

Academic Editor: Michele Bernasconi

Received: 19 August 2021
Accepted: 30 August 2021
Published: 5 September 2021

Publisher's Note: MDPI stays neutral with regard to jurisdictional claims in published maps and institutional affiliations.



Copyright: © 2021 by the authors. Licensee MDPI, Basel, Switzerland. This article is an open access article distributed under the terms and conditions of the Creative Commons Attribution (CC BY) license (<https://creativecommons.org/licenses/by/4.0/>).

Simple Summary: Preclinical analyses identified APR-246 as a potent treatment option for neuroblastoma. However, a specific mode of action, sufficient biomarkers and promising combination partners are still missing. Here, we analyze the susceptibilities of different entities and relate them to gene expression profiles and previously described biomarkers. We propose a gene signature, consisting of 13 genes, as a novel predictive biomarker. Furthermore, we provide evidence that APR-246 directly targets metabolic weaknesses in neuroblastoma cell lines, thus hampering ROS detoxification. This makes APR-246 suitable to be combined with ROS-inducing HDAC inhibitors, a treatment combination that has not been described for neuroblastoma thus far.

Abstract: APR-246 (Eprenetapopt/PRIMA-1^{Met}) is a very potent anti-cancer drug in clinical trials and was initially developed as a p53 refolding agent. As an alternative mode of action, the elevation of reactive oxygen species (ROS) has been proposed. Through an in silico analysis, we investigated the responses of approximately 800 cancer cell lines (50 entities; Cancer Therapeutics Response Portal, CTRP) to APR-246 treatment. In particular, neuroblastoma, lymphoma and acute lymphocytic leukemia cells were highly responsive. With gene expression data from the Cancer Cell Line Encyclopedia (CCLE; $n = 883$) and patient samples ($n = 1643$) from the INFORM registry study, we confirmed that these entities express low levels of *SLC7A11*, a previously described predictive biomarker for APR-246 responsiveness. Combining the CTRP drug response data with the respective CCLE gene expression profiles, we defined a novel gene signature, predicting the effectiveness of APR-246 treatment with a sensitivity of 90% and a specificity of 94%. We confirmed the predicted APR-246 sensitivity in 8/10 cell lines and in ex vivo cultures of patient samples. Moreover, the combination of ROS detoxification-impeding APR-246 with approved HDAC-inhibitors, known to

elevate ROS, substantially increased APR-246 sensitivity in cell cultures and in vivo in two zebrafish neuroblastoma xenograft models. These data provide evidence that APR-246, in combination with HDAC-inhibitors, displays a novel potent targeted treatment option for neuroblastoma patients.

Keywords: histone deacetylases; ROS; TP53; small molecule inhibitors; pediatric tumors of the nervous system; precision medicine; response prediction biomarker

1. Introduction

Neuroblastoma is the most common extracranial solid tumor in childhood, accounting for 15% of pediatric cancer mortality [1]. Clinical characteristics of neuroblastoma cases are highly diverse concerning tumor size, progression, therapeutic response and prognosis. Treatment is implemented according to the respective risk group [2,3]. For low and intermediate risk tumors, which in general have a good prognosis, treatment ranges from observation and surgical resection to chemotherapy or radiation. Despite the intense therapeutic approach for high-risk neuroblastoma, the outcome is still poor, indicating a medical need for novel treatment options [4].

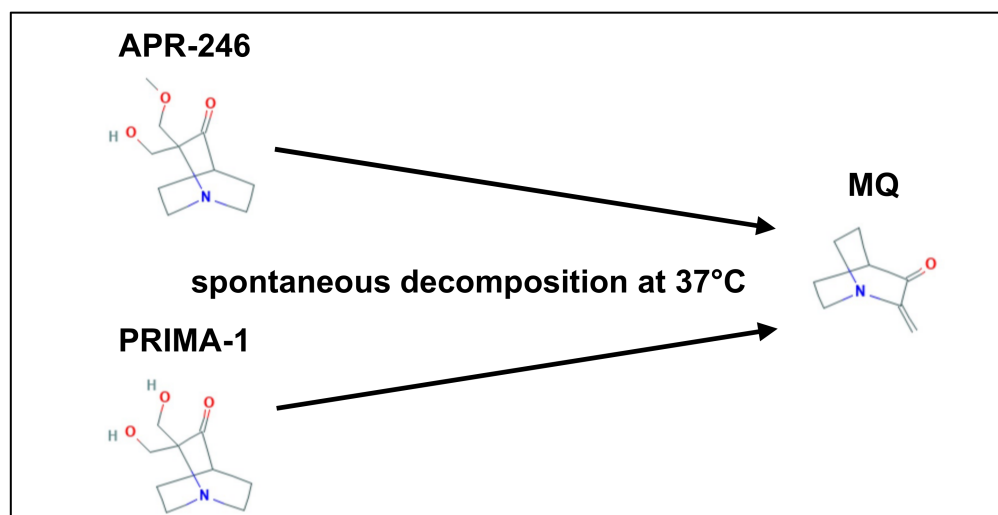
The tumor suppressor gene *TP53* is mutated in approximately 50% of all human cancers and to some extent nearly all cancers develop the ability to circumvent p53 pathway activation [5]. Primary neuroblastomas only rarely display *TP53* mutations, whereas relapsed high-risk neuroblastomas frequently show *TP53* mutations and loss of p53 function, which are both linked to a poor prognosis [6–9].

Over the last 20 years, novel drugs were developed to reactivate mutated p53 [10]. The most advanced drug is APR-246, which is currently being tested in 12 clinical trials [11]. A phase III clinical study is assessing the efficacy of APR-246 in combination with azacytidine (NCT03745716). APR-246 is showing a very promising clinical potential, with a maximum plasma concentration of approximately 280 μM and a half-life of four to five hours, which corresponds to an estimated trough plasma concentration of 15–20 μM [12–14]. APR-246 is the methylated functional analogue of PRIMA-1, which was discovered in a cellular viability screening with an inducible expression system for mutant *TP53* in *TP53* knockout SAOS-2 cells [15]. Subsequent cell culture studies demonstrated that the prodrugs PRIMA-1 and APR-246 are converted spontaneously to reactive methylene quinuclidine (MQ) (Scheme 1) [16]. MQ covalently binds to cysteine residues of the mutant p53 (namely cysteine 124 and 277), which changes the protein's conformation. This restores its DNA-binding function and induces a strong apoptotic signal [15,17].

In addition, MQ is able to bind other cysteine residues, e.g., thioredoxin reductase 1 (TrxR1) and glutathione [18,19]. MQ bound TrxR1 increases the ROS level via converting the enzyme to a pro-oxidant NADPH oxidase [18]. The tripeptide glutathione consists of glycine-cysteine-glutamate, of which cysteine is the active amino acid that is responsible for its antioxidant function. MQ binding impairs the antioxidant glutathione system and thus elevates the levels of reactive oxygen species (ROS) and lipid peroxidation, thereby promoting cell death [19]. Cysteine importers, such as SLC7A11 (also commonly known as xCT), are responsible for the intracellular amount of cysteine, and thus glutathione [19]. *SLC7A11* gene expression was identified as a response prediction biomarker for APR-246 treatment in esophagus carcinoma cell lines, whereby low expression levels of the cysteine importer are associated with a higher response to APR-246 treatment [19].

It is well-known that ROS levels can increase with cancer progression, for example through the induction of replicative stress [20]. In this case, elevated ROS levels can cause novel vulnerability in relapsed malignancies, i.e., in MAPK inhibitor resistant melanoma cells. In these cells, histone deacetylase (HDAC) inhibitors substantially elevated ROS levels and sensitized resistant cells for MAPK inhibitor treatment [21]. The enzyme family of HDACs is linked to oncogenic events and plays a major role in pediatric cancers of the nervous system [22–26]. Hence, HDAC inhibitors have demonstrated antitumor effects in

various pediatric tumor models [27–33]. To date, several HDAC inhibitors are approved for the treatment of hematological cancers (e.g., vorinostat for cutaneous T-cell lymphoma and Panobinostat for multiple myeloma) and several clinical trials are investigating HDAC inhibitors as both single agents and in combination with chemotherapeutics, for additional tumor entities [34–36].



Scheme 1. APR-246 and PRIMA-1 are prodrugs that are both spontaneously converted to highly reactive MQ in enzyme-free conditions [37–39].

With this study, we aimed to investigate the effectiveness of APR-246 in the treatment of pediatric nervous system tumors in order to test and optimize predictive biomarkers and to show that ROS detoxification-impeding APR-246 is a promising potential combination partner for the ROS elevating HDAC inhibitors.

2. Materials and Methods

2.1. Cell Culture

Cell lines were cultured at 37 °C in a humidified atmosphere with 5% CO₂. DNA fingerprinting authentication (DSMZ, Braunschweig, Germany) and bacterial and viral (including mycoplasma) contaminations were regularly checked (Multiplexion, Heidelberg, Germany). Adherent cell lines were detached using Trypsin (Gibco, Thermo Fisher Scientific Inc., Waltham, MA, USA).

The following neuroblastoma cell lines (all passage < 30) were cultured in Dulbecco's Modified Eagle Medium (DMEM, Gibco, Thermo Fisher Scientific Inc., Waltham, MA, USA) with L-Glutamine supplemented with 10% fetal calf serum (FCS, Sigma-Aldrich, Munich, Germany) and 1% non-essential amino acids (NEAA, Lonza, Basel, Switzerland): SK-N-BE(2)-C (European Collection of Cell Cultures, ECACC), IMR-32 (German Collection of Microorganisms and Cell Cultures, DSMZ, Darmstadt, Germany), SK-N-AS (kindly provided by M. Schwab, DKFZ, Heidelberg, Germany), SH-SY5Y (DSMZ, Darmstadt, Germany), SK-N-FI (kindly provided by F. Westermann, DKFZ, Heidelberg, Germany), Kelly (DSMZ, Darmstadt, Germany), IMR5/75 (kindly provided by F. Westermann, DKFZ, Heidelberg, Germany), SIMA (kindly provided by F. Westermann, DKFZ, Heidelberg, Germany), SH-EP (passage 15 to 30, kindly provided by F. Westermann, DKFZ, Heidelberg, Germany), SK-N-BE(2) (passage 15 to 30, DSMZ, Darmstadt, Germany) and NB-1 (passage 15 to 30, RIKEN Cell Bank, Japan) were cultured using RPMI 1640 with L-Glutamine (Gibco, Thermo Fisher Scientific Inc., Waltham, MA, USA), 10% FCS, 1% NEAA.

Vincristine resistant and non-resistant SK-N-BE(2)-C (passage 30 to 45, kindly provided by M. Michaelis, University of Kent, and J. Cinatl, Goethe University, Frankfurt am Main) were cultured using IMDM with L-Glutamine, 2 mM HEPES (Gibco, Thermo Fisher Scientific Inc., Waltham, MA, USA) supplemented with 10% FCS; for the resistant

cells, 20 ng/mL vincristine was added to the medium. The cells were made to be resistant to vincristine-treatment through long-term cultivation in a vincristine containing medium [40].

The following pediatric high-grade glioma cell lines were used: SJ-GBM2 (passage 30 to 45, DMEM, 10% FCS, 1% NEAA), KNS-42 (passage 55 to 70, DMEM, 10% FCS, 1% NEAA), and SF188 (passage 95 to 110, DMEM, 10% FCS).

For the culture of Δ 6RT 3T3 and C5-Gl 3T3 (passage 5 to 20 after obtaining, kindly provided by D. Pestov, Department of Cell Biology and Neuroscience, Rowan University School of Osteopathic Medicine, Stratford, NJ, USA), DMEM supplemented with 10% FCS was used [41].

The T-cell leukemia cell line Jurkat (passage 5 to 15 after obtaining, kindly provided by J. Hoheisel, DKFZ, Heidelberg, Germany) was cultured using RPMI 1640 with L-Glutamine (Gibco, Thermo Fisher Scientific Inc., Waltham, MA, USA), 10% FCS, 1% NEAA. The ALL cell lines NALM-6 (passage 5 to 15 after obtaining, kindly provided by T. Grünewald, DKFZ, Heidelberg, Germany) and REH (passage 5 to 15, kindly provided by T. Grünewald, DKFZ, Heidelberg, Germany) and the B-cell lymphoma cell line Jeko-1 (passage 5 to 15, kindly provided by M. Persicke, lab of D. Mertens, DKFZ, Heidelberg, Germany) were cultured using RPMI 1640 with L-Glutamine (Gibco, Thermo Fisher Scientific Inc., Waltham, MA, USA) supplemented with 10% FCS (Sigma-Aldrich, Munich, Germany). The T-cell lymphoma cell line HuT 78 was cultured with IMDM with L-Glutamine, and 2 mM HEPES (Gibco, Thermo Fisher Scientific Inc., Waltham, MA, USA) supplemented with 20% FCS.

Long-term cultures (LTC) were established from primary tumor samples obtained through the INFORM study (INdividualized Therapy FORe Relapsed Malignancies in Childhood [42]). The cells (passage 15 to 30 after isolation from the original tumor) were cultured using Tumor Stem Medium (TSM; [43]). The TSM consisted of filtered (Stericup-GP 500 mL Express Plus PES 0.22 μ m, Merck, Darmstadt, Germany) TSM Base Medium (47.5% Neurobasal-A Medium, 47.5% D-MEM/F-12, 1% HEPES Buffer Solution (1 M), 1% sodium pyruvate MEM 100 MM(CE), 1% MEM Non-Essential Amino Acids Solution 10 mM, L-glutamine solution BIOXTRA, 2 mM, 1% Penicillin-Streptomycin-Glutamine, Life Technologies, Thermo Fisher Scientific Inc.) supplemented with 2% B27 Supplement Minus Vitamin A (50 \times , Life Technologies, Thermo Fisher Scientific Inc., Waltham, MA, USA), 0.02% (*w/v*) recombinant human EGF (100 μ g/mL, PeproTech Inc., Rocky Hill, NJ, USA), 0.02% (*w/v*) recombinant human FGF-basic (100 μ g/mL, PeproTech Inc., Rocky Hill, NJ, USA), 0.05% H-PDGF-AA (20 μ g/mL, PeproTech Inc., Rocky Hill, NJ, USA) and 0.1% Heparin Solution (2 mg/mL, Sigma-Aldrich, Munich, Germany). The following cultures from INFORM patient samples were used: INF_R_1288_LTC, rhabdoid tumor (ATRT, MYC by methylation profiling); INF_R_1467_LTC, soft tissue sarcoma (eRMS by methylation profiling); INF_R_1490_LTC, osteosarcoma (OS_HG by methylation profiling) and INF_R_1632_PDX_LTC, neuroblastoma (NB, MYCN by methylation profiling). Ethics committee approval for INFORM was obtained from Heidelberg University Hospital's review board.

Isolation and long-term cell culture establishment of PDX_LTC cells: INF_R_1632_PDX cells were isolated from a subcutaneous patient-derived xenograft (PDX) model established with a fresh surgical specimen of an INFORM patient with relapsed neuroblastoma according to a protocol adapted from Stewart et al. [44]. One tumor-bearing mouse was sacrificed when the volume of the subcutaneous tumor reached approximately 500 mm³. The harvested tumor tissue (260 mg) was minced thoroughly with sterile scissors, and was subsequently enzymatically digested for 10 min at 37 °C by incubating it with 1.2 μ g/mL trypsin (Sigma-Aldrich, Munich, Germany) in Neurobasal-A medium (Life Technologies, Thermo Fisher Scientific Inc., Waltham, MA, USA). The reaction was stopped by adding 1.2 μ g/mL trypsin inhibitor (Sigma-Aldrich, Munich, Germany), followed by the repeated stepwise addition of 60 μ L 1 mg/mL DNase in 0.5 M MgCl₂ until viscosity of the solution was decreased, such that remaining tumor fragments easily settled to the bottom of the tube. After passing the cell suspension through a 40 μ m cell strainer (Corning, Corning,

NY, USA), the cells were spun down at 500 g for 10 min at room temperature. Red blood cells were removed by two cycles of 2 min incubation of the cell pellet in 2 mL ACK Lysing buffer (Lonza, Basel, Switzerland) at room temperature, followed by washing with a TSM base medium. The cells were taken into culture in TSM complete medium and formed free-floating three-dimensional spheroids and semi-adherent spheroids within 24 h after tumor dissociation. Free-floating and semi-adherent spheroids were dissociated with TrypL Express (Life Technologies, Thermo Fisher Scientific Inc., Waltham, MA, USA; 5 min, 37 °C) when they reached a size of 700–1000 µm, and the cells were sub-cultured at a ratio of 1:3 to 1:5 in fresh TSM complete. When the cells reached cell passage six, they were considered to be established and long-term cultures (INF_R_1632_PDX_LTC); we did not observe an obvious slowdown in cell growth over at least 35 passages in culture.

2.2. Chemicals

The following Table 1 summarizes the chemicals, reagents and diluents used.

Table 1. Chemicals, reagents and diluents used.

Name	Company	Stock Conc., Diluent
APR-246	Selleck Chemicals, Munich, Germany	50 mM, DMSO
doxorubicin	Biozol, Eching, Germany	10 mM, H ₂ O
vincristine	Enzo Life Sciences, Lörrach, Germany	10 mg/mL, DMSO
vorinostat	Selleck Chemicals, Munich, Germany	100 mM, DMSO
entinostat	Biomol GmbH, Hamburg, Germany	10 mM, DMSO
abexinostat	Selleck Chemicals, Munich, Germany	10 mM, DMSO
Panobinostat	Cayman Chemical, Hamburg, Germany	0.5 mM, DMSO
romidepsin	Biovision Inc., Milpitas, CA, USA	1 mM, DMSO
H ₂ O ₂	Sigma-Aldrich, Munich, Germany	30% w/w H ₂ O
DMSO	Sigma-Aldrich, Munich, Germany	-

2.3. Western Blot

Western blot analysis was performed as previously described [28]. The primary antibodies anti-p53 (sc-126, Santa Cruz Biotechnology, Dallas, TX, USA) and anti-GAPDH (JC1682928, Millipore, Darmstadt, Germany) were used. Peroxidase conjugated goat anti-mouse IgG (Fc specific) antibodies (A-0168, Sigma-Aldrich, Munich, Germany) were used as secondary antibodies. The original Western Blots data was shown in the Supplementary Materials.

2.4. Real-Time PCR

Real-time PCR was performed as described previously [45,46]. The following primers were purchased from ThermoFisher Scientific, Waltham, MA, USA:

CDKN1A (*p21^{WAF1/CIP1}*, forward: 5'-TGG AGA CTC TCA GGG TCG AAA-3', reverse: 5'-GGC GTT TGG AGT GGT AGA AAT C-3'), *HPRT* (forward: 5'-TGA CAC TGG CAA AAC AAT GCA-3', reverse: 5'-GGT CCT TTT CAC CAG CAA GCT-3'), *SDHA* (forward: 5'-TGG GAA CAA GAG GGC ATC TG-3', reverse: 5'-CCA CCA CTG CAT CAA ATT CAT G-3'), and *PUMA* (forward: 5'-CCT GGA GGG TCC TGT ACA ATC T-3', reverse: 5'-GCA CCT AAT TGG GCT CCA TCT-3'). The primer for *GADD45A* was purchased from Qiagen, Hilden, Germany (QT00014084). The delta-delta-Ct method was used to calculate the relative expression, and normalization was performed to neuroblastoma specific housekeeping genes *SDHA* and *HPRT* [45,47].

2.5. Flow Cytometry Analysis

Flow Cytometry was applied to analyze the lipid peroxidation (BODIPY staining) and to detect ROS (DCFDA staining).

BODIPY 581/591 C11 Lipid peroxidation sensor staining (stock concentration: 20 mM in dimethylformamide, Invitrogen, Thermo Fisher Scientific, Waltham, MA, USA) was

used at a working concentration of 20 μM , and was diluted with RPMI without phenol red (Gibco, Thermo Fisher Scientific Inc., Waltham, MA, USA). After inspection, the cells were detached, centrifuged and stained for 20 min at 37 °C in a 500 μL staining solution. After centrifugation, cells were resuspended in 300 μL RPMI without phenol red, supplemented with 10% FCS. Fluorescence was measured in a FACSCanto II (BD) with 488 nm excitation and detected using a 502 nm longpass and 530/30 nm bandpass filter. Data were analyzed using FlowJo 10.x (FlowJo LLC, Ashland, OR, USA).

ROS detection was performed as previously described [27].

2.6. Metabolic Activity Assays

If not otherwise declared, cells were precultured for 72 h at a density of 2,000,000 cells per T75 flask (exceptions: Kelly, NB1 and IMR-32 4,000,000 per T75 flask, SJ-GBM2 1,000,000 per T75 flask). Cells were detached with trypsin—EDTA (Thermo Fisher Scientific, Waltham, MA, USA) and seeded in 96-well plates (Greiner, Microplate, 96-Well, PS, F-bottom $\mu\text{CLEAR}^{\text{®}}$, CELLSTAR $^{\text{®}}$) in 100 μL medium per well at a density of 5000 (KNS-42, SJ-GBM2, SF188, SK-N-BE(2)-C) or 10,000 (IMR-32, NB1, Kelly) cells/well. HDAC-inhibitor screenings were performed accordingly in 384-well plates (Greiner, Microplate, 384-Well, PS, F-bottom $\mu\text{CLEAR}^{\text{®}}$, CELLSTAR $^{\text{®}}$) in 20 μL medium per well at a density of 1250 (SK-N-BE(2)-C, SK-N-AS) or 2500 (IMR-32) cells/well. To avoid edge effects, margin wells (row A and H, column 1 and 12) contained PBS or medium and medium-containing wells were used as background controls. After 24 h incubation, cells were treated for 72 h. Drugs were applied using a Tecan D300e drug printer. Cell viability was quantified using CellTiter-Glo $^{\text{®}}$ 2.0 kit (Promega, Madison, WI, USA). 50 μL CellTiter-Glo $^{\text{®}}$ (96-well) or 25 μL CellTiter-Glo $^{\text{®}}$ (384-well) were added to every well, the plates were shaken at 400 rpm for 5 min and were then incubated for another 10 min. Bioluminescence was quantified on an OPTIMA plate reader (BMG Labtech, Ortenberg, Germany).

2.7. Trypan Blue Assay

An automated Trypan Blue Assay was performed as previously described [30].

2.8. Zebrafish Lines

The care for and breeding of the zebrafish were done under standardized conditions, as described previously [48]. Zebrafish wild-type AB line was raised at 28 °C. Embryos used for tumor injections were maintained in an E3 buffer supplemented with 0.2 mM 1-phenyl-2-thiourea (PTU, Sigma, Munich, Germany).

2.9. Cell Preparation for Zebrafish Embryo Xenotransplantation

Cell preparation and xenotransplantation were performed as described previously [48]. Briefly, cells (NB-1 and IMR-32) were cultured to 70–80% confluence, and then harvested and labeled with CellTracker CM-DiI (Thermo Fisher Scientific, Waltham, MA, USA). To minimize cell clumping, DNase I (250 Kunitz units/mL, Sigma-Aldrich, Munich, Germany) for IMR-32 and Benzonase (E1014-25KU, Sigma-Aldrich, Munich, Germany) for NB-1 was added to the cell suspension and washed twice with 10% FCS RPMI, twice with serum-free RPMI and resuspended in serum-free RPMI to a final concentration of 1.0×10^8 cell/mL. Zebrafish embryos were anesthetized with tricaine (MS-222, 3-Amino-benzoäure-ethylester-methansulfonat, 0.02% (*w/v*), Sigma-Aldrich, Munich, Germany) and embedded in 1.0% of low gelling temperature agarose (Sigma-Aldrich, Munich, Germany). 150 to 250 CM-DiI-labeled tumor cells were injected into the yolk sac of each embryo using a FemtoJet express microinjector (Eppendorf, Hamburg, Germany) and glass microinjection needles (Science Products, Hofheim, Germany). Shortly (30 min) after injection, embryos were transferred to and held at 34 °C.

2.10. Zebrafish Embryo Drug Toxicity Assay

The toxicity of the compounds was assessed before performing *in vivo* experiments and a Maximum Tolerated Dose (MTD) was determined. Embryos (48 hpf) were transferred to 48-well uncoated plates (Corning, Corning, NY, USA) containing different concentrations of the compounds and a solvent control. The stock solution of the compounds was further dissolved in E3 buffer supplemented with 0.2 mM 1-phenyl-2-thiourea (PTU, Sigma, Munich, Germany) in order to reach the desired concentrations. Three embryos were tested per concentration or solvent control. Embryos were kept at 34 °C during the experiment and were imaged at 72 hpf and 120 hpf using a stereo microscope (Leica). The embryos were assessed for signs of toxicity, such as death, morphology changes (curvature of body, edema) and behavioral changes. APR-246 concentration range tested: 10–200 µM, MTD: 50 µM; solvent control: DMSO (0.2% and 0.5%); Vorinostat concentration range tested: 2.5–100 µM, no toxicity detected (MTD: 100 µM); solvent control: DMSO (0.1%).

2.11. Zebrafish Embryo Drug Treatment and Efficiency Evaluation

Drug treatment and efficiency evaluation were performed as described previously [48]. Briefly, embryos with tumor xenografts, detected by red signals in fluorescence microscopy (Nikon, Tokyo, Japan) 2 h post implantation, were transferred to 48-well uncoated plates (Corning, Corning, NY, USA). Then, embryos were incubated in freshly prepared E3 medium supplemented with 1% N-Phenylthiourea (PTU, Sigma-Aldrich, Munich, Germany) containing drugs or solvent control. Tumor growth was evaluated by confocal microscopy before drug exposure and 48 h post treatment (Zeiss LSM 710 confocal microscope (Zeiss, Oberkochen, Germany) and ZEN software (Zeiss, Oberkochen, Germany)). The responses of tumor volumes were categorized according to the Response Evaluation Criteria in Solid Tumors (RECIST) 1.1, which was adopted for zebrafish tumors, to visualize best response: progressive disease (PD, at least a 20% increase in tumor volume), stable disease (SD, neither sufficient shrinkage to qualify for PR nor sufficient increase to qualify for PD), and partial response (PR, at least a 30% decrease in tumor volume).

2.12. *In Silico* Data Analysis and Genetic Signature Generation

We downloaded drug response data for $n = 1107$ cell lines to PRIMA-1 from the Cancer therapeutics response CTD² portal (Broad Institute, Cambridge, MA, USA, CTRP v2, 2015) [49–52]. The data were combined with gene expression and *TP53* mutation data for the respective cell lines and entities from the Cancer Cell Line Encyclopedia (CCLE, Broad Institute, Cambridge, MA, USA, $n = 883$ from 1375 CCLE cell lines had *TP53* data on the CTRP); doublets were excluded. We first used drug response data to discriminate between the cell lines that were responsive (area under curve below 11, reflecting an app. IC₅₀ of less than 10 µM, $n = 102$ cell lines) and less-responsive (area under curve above 13, reflecting an app. IC₅₀ of more than 40 µM, $n = 303$ cell lines) to PRIMA-1 treatment. We then looked for differentially expressed genes in the responsive versus less-responsive cohorts using the Cancer Cell Line Encyclopedia (CCLE, Broad Institute, Cambridge, MA, USA) gene expression data set in R2 (R2: microarray and visualization platform: <http://r2.amc.nl>, accessed on 5 January 2021).

Using z-scores of log₂ transformed gene expression data, we identified $n = 171$ genes as the most significantly differentially expressed genes between the two cohorts (p -value < 2.82×10^{-31} , $n = 16$ upregulated and $n = 155$ downregulated genes). We tested every gene on this list for its suitability as a single gene predictive biomarker against the whole CCLE cohort. Downregulated genes were characterized by a negative overall fold change; upregulated genes were characterized by a positive overall fold change. Whether a gene in a respective cell line was up- or downregulated was reflected by its z-score. Based on how often these predictions were true, we calculated the sensitivity (true positive prediction rate), specificity (true negative prediction rate) and general false prediction rate using an R script (Supplementary Materials).

To investigate the predictive power of the combinations of several genes, we first analyzed the up- and downregulated genes separately:

For upregulated genes ($n = 16$), we tested every possible combination of genes by calculating the sum of the z-scores for every cell line. We assumed that positive and negative sums of z-scores would predict the responders and low-responders, respectively. We then calculated the sensitivity, specificity and false prediction rate by comparing the number of predicted responders and low-responders to the actual responder vs. low-responder status. The best combination, with 84.3% sensitivity, 96.7% specificity and a 5.0% false prediction rate, was then used for the ratio calculation described below.

Due to the high number of downregulated genes ($n = 155$), we analyzed a limited number of 40 downregulated genes: 20 with the lowest false prediction rate and 20 with the highest sensitivity from the single gene analysis. These 40 genes were combined in every possible way up to a group size of five. Sensitivity and specificity of every combination were calculated under the following assumptions: A negative sum of z-scores predicted responders and a positive sum of z-scores predicted low-responders. Predictions and true responder/low-responder status were compared. Based on the number of correctly predicted responder and low-responder sensitivity, specificity and false prediction rate were calculated. The best combination, with 90.2% sensitivity, 94.7% specificity and a 5.0% false prediction rate, was then used for the ratio calculation.

To merge the best above identified combinations of down- and upregulated genes, we divided the sum of the upregulated gene expression values (log₂ transformed) by the sum of downregulated gene expression values (log₂ transformed). To identify a cut-off value for the discrimination of responders from low-responders, we used the receiver operating curve (ROC) analysis (ROCR R-package). Samples with a ratio > ROC cut-off are predicted as responders, samples with a ratio < cut-off are predicted as low-responders. The R-package compared the prediction to real response from the Cancer Therapeutics Response Portal and calculated the sensitivity, specificity and false prediction rate.

By using the ratio of log₂ transformed gene expression values of the respective genes, it was possible to calculate a genetic signature score (“biomarker”) for any cohort of interest (e.g., INFORM).

2.13. Stastical Analyses

All cell culture experiments were performed in triplicate. A two-tailed *t*-test, unpaired or paired, or ANOVA where appropriate, were performed using software program R (R version 3.2.2, 2015; The R Foundation for Statistical Computing). The packages tidyverse, janitor, readxl, writxl, ROCR, ggplot2 and ggsignif were used to calculate and plot the data. *p*-values of less than 0.05 were considered significant (* $p < 0.05$, ** $p < 0.01$, *** $p < 0.001$). IC₅₀ values were calculated using GraphPad Prism Version 9.1.0 (GraphPad Software, San Diego, CA, USA). Synergistic interactions were analyzed with SynergyFinder using the HSA (highest single agent) reference model, as the assumptions of other models were not fulfilled [53].

3. Results

3.1. Pure TP53 Mutation Status Is Not a Sufficient Biomarker for APR-246 Sensitivity of Pediatric Tumors of the Nervous System

While developed as a p53 stabilizing agent, it has emerged that TP53’s mutation status alone is not a satisfactory biomarker for APR-246/PRIMA-1 sensitivity, e.g., in Ewing sarcoma and esophagus carcinoma models [54,55]. To investigate APR-246/PRIMA-1 responsiveness and the predictive value of the TP53 mutation status for childhood tumors, we applied in silico data analysis. We combined the data for the TP53 mutation status of a large cohort of cancer cell lines (including pediatric entities such as medulloblastoma, neuroblastoma and Ewing sarcoma) from the Cancer Cell Line Encyclopedia (CCLE, Broad Institute, Cambridge, MA, USA) and the DepMap portal with PRIMA-1 sensitivity data obtained from the CTD² portal (Broad Institute, Cambridge, MA, USA,

CTRP v2, 2015) [49,56,57]. If the *TP53* mutation type was the main driver of responsiveness, sensitivity to PRIMA-1/APR-246 would be expected in cell lines that harbor *TP53* point mutations leading to a conformational change impairing DNA binding, as this can be reversed by APR-246/PRIMA-1 [14–16]. These include the missense mutations R273H, R273C, C135F and G266E [58]. In line with the studies mentioned above, our analysis revealed no increased sensitivity in cell lines (total as well as pediatric-only) harboring these missense mutations (Figure 1a, Figure S1).

Moreover, the wet-lab results from five pediatric tumor cell lines treated with APR-246 proved no correlation of IC50 values with the *TP53* mutation status. In fact, the *TP53* wild type cell line (IMR-32) was the most sensitive of all tested cell lines, as determined by metabolic activity readout (Table 2). We used three cell lines that harbor common *TP53* missense mutations within their DNA-binding domain (R273C, G266E and C135F), one cell line with a nonsense mutation (R342*, DNA-binding function remains intact), and one *TP53* wild-type cell line (Table 2). The Western blot analysis revealed the accumulation of p53 protein, which is typical for *TP53* mutation, for SJ-GBM2 (R273C), SF188 (G266E) and SK-N-BE(2)-C (C135F) cells (Figure 1b). To further investigate the contribution of p53 for APR-246 sensitivity, we treated NIH3T3-*TP53* knockout cells and the corresponding NIH3T3-*TP53* wild-type cells with APR-246. Both cell types equally responded to APR-246 treatment, independently of the *TP53* status (Table 2).

Table 2. Sensitivity to APR-246 in five different pediatric tumor cell models of the nervous system, measured via metabolic activity (CTG).

Cell Line	Entity/ <i>TP53</i> Status	IC50/95% CI [μ M]
SJ-GBM2	pHGG ¹ /mut, p.R273C	71.8/69.3–74.4
SF188	pHGG/mut, p.G266E	43.9/39.4–48.8
KNS-42	pHGG/mut, p.R342 ^{*2}	27.8/22.8–33.7
SK-N-BE(2)-C	neuroblastoma/mut, p.C135F	24.7/22.0–27.7
IMR-32	neuroblastoma/wt	4.0/3.2–4.8
NIH-3T3 C5-GL (<i>TP53</i> ko)	murine embryo fibroblasts	18.4/15.8–21.3
NIH-3T3 Δ 6RT (<i>TP53</i> wt)	murine embryo fibroblasts	18.7/17.6–19.9

¹ pediatric high-grade glioma. ² nonsense mutation (*) affecting the tetramerization domain, not the DNA binding domain of p53.

To determine whether APR-246 exerts its p53-activating potential, we combined APR-246 with doxorubicin, which is a well-known DNA damage and p53 response inducer. Doxorubicin single-treatment activated p53 in the *TP53*-wt cell line IMR-32, as indicated by the upregulation of the p53 target genes *CDKN1A*, *PUMA* and *GADD45A* (Figure 1c; Figure S2). The addition of APR-246 to doxorubicin treatment did not increase target gene expression in the *TP53*-wildtype setting when compared to cells treated with doxorubicin only (Figure 1c; Figure S2). In the *TP53* mutant neuroblastoma cell line SK-N-BE(2)-C (C135F), doxorubicin single treatment failed to activate p53 target gene expression. Furthermore, the addition of APR-246 to doxorubicin did not improve p53 target gene induction in this cell line (Figure 1d; Figure S2). Nevertheless, when combining a fixed APR-246 concentration with different doses of doxorubicin, we observed increased doxorubicin sensitivity in both the *TP53*-wt IMR-32 cell line (Figure 1e) and in the doxorubicin resistant *TP53*-mutant SK-N-BE(2)-C cell line (Figure 1f). Our metabolic activity data thus suggest that the combination of APR-246 with doxorubicin reduces viability in both *TP53*-wt and mutant neuroblastoma cell lines, despite the absence of a p53 target gene expression response in the *TP53*-mutant cell line.

These findings were confirmed in *TP53* mutant pHGG cell lines SJ-GBM2 and SF188 (Figure 1g–h). Similar to SK-N-BE(2)-C cells, both cell lines exhibited decreased cell viability upon doxorubicin treatment combined with APR-246. Again, we observed no reactivation of p53 target gene expression (*CDKN1A* and *GADD45A*) upon APR-246 treatment in these cells (Figure S3). Altogether, these results suggest that the *TP53* mutation status alone is

not sufficient to predict the response to APR-246 alone or in combination with doxorubicin in childhood tumors of the nervous system.

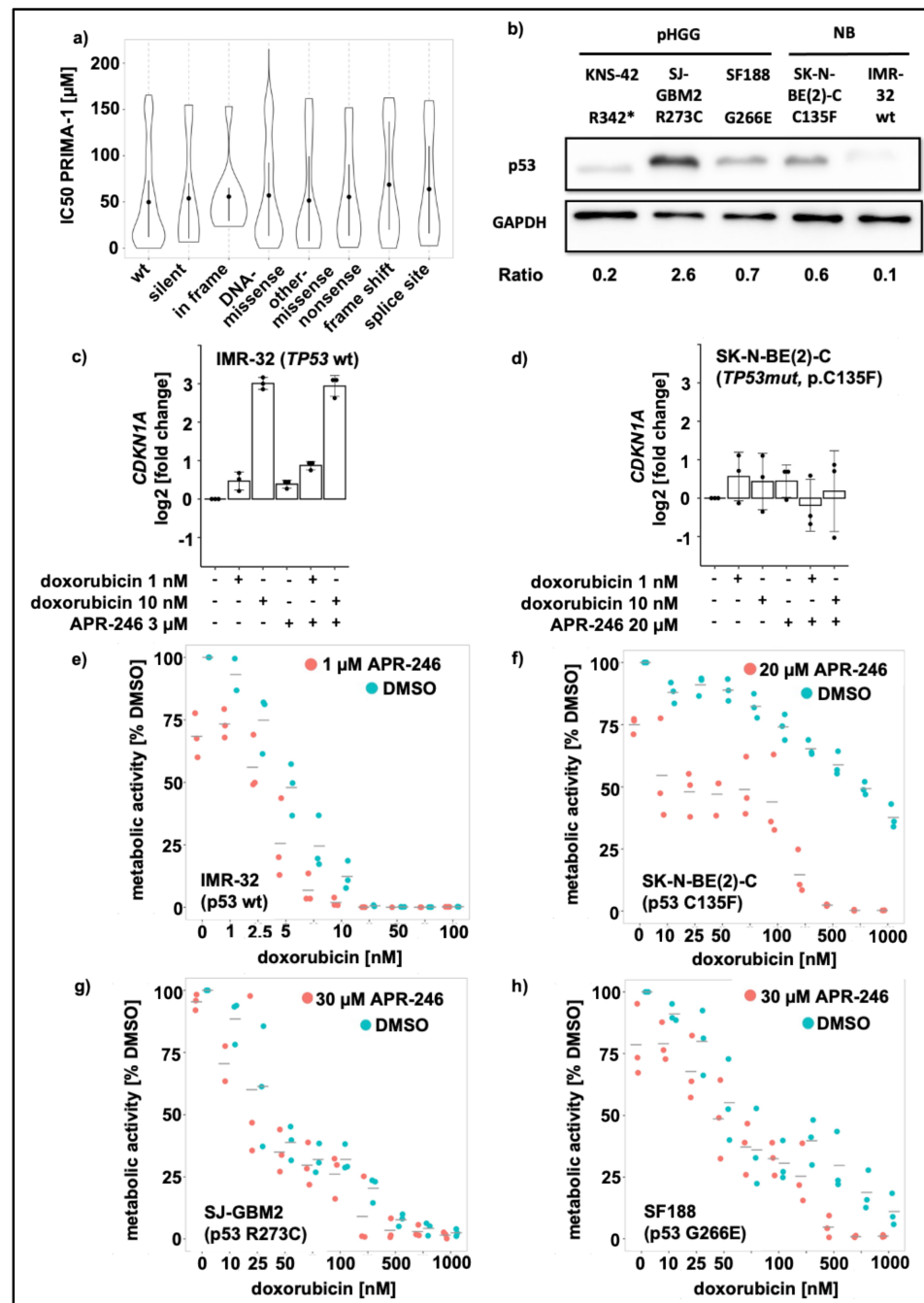


Figure 1. TP53 mutation status insufficiently predicts the APR-246/PRIMA-1 response. (a): PRIMA-1 sensitivity separated according to TP53 mutation status derived from Cancer Cell Line Encyclopedia and CTD² portal ($n = 805$); (b): Expression of p53 is shown in the Western blot of the whole cell lysates of one TP53 nonsense mutated cell line (KNS-42), three TP53 missense mutated cell lines (SJ-GBM2, SF188, SK-N-BE(2)-C) and one TP53 wild type cell line (IMR-32). GAPDH served as loading control. The ratio indicates normalization of p53 to the GAPDH signal; (c,d): RT-PCR measurement of TP53 pathway activation. CDKN1A expression is depicted as log₂ transformed fold change to solvent control. Treatment was applied for 24 h with doxorubicin or APR-246, alone or in combination, as indicated; (e,f): metabolic activity measurement with CellTiter Glo-assay in neuroblastoma cell lines IMR-32 (e) and SK-N-BE(2)-C (f) after 72 h treatment. IMR-32 (e) were treated with 0–100 nM

doxorubicin alone (blue) or in combination with a fixed APR-246 concentration of 1 μ M (red). SK-N-BE(2)-C (f) were treated with 0–1000 nM doxorubicin alone (blue) or in combination with a fixed APR-246 concentration of 20 μ M (red). Luminescence was normalized to the solvent control (DMSO). (g,h): metabolic activity measurement with CellTiter Glo-assay in pediatric high-grade glioma cell lines SJ-GBM2 (g) and SF188 (h) upon 72 h treatment. Both were treated with 0–1000 nM doxorubicin alone (blue) or in combination with a fixed APR-246 concentration of 30 μ M (red). Luminescence was normalized to the solvent control (DMSO).

3.2. APR-246 Impairs Oxigene Species Elimination and Basal Reactive Oxygen Species Level Indicate APR-246 Sensitivity

Besides binding to mutant p53, the APR-246/PRIMA-1 product MQ has been described to covalently bind to and inactivate the antioxidant tripeptide glutathione [19]. Additionally, MQ has been shown to inhibit thioredoxin reductase 1 (TrxR1) resulting in a pro-oxidant NADPH-oxidase [18]. These effects result in increased levels of reactive oxygen species (ROS) [18,19]. We observed increased ROS formation and lipid peroxidation in our neuroblastoma models upon APR-246 treatment (Figure 2a,b). In addition, we compared basal ROS levels of responsive IMR-32 as well as less responsive SK-N-BE(2)-C and SJ-GBM2 cells. Whereas the sensitive IMR-32 cells displayed very high basal ROS levels, the less-responsive cell lines exhibited only low basal ROS levels, suggesting that cells with a high degree of basal oxidative stress respond better to the treatment (Figure 2c). To test this assumption, we analyzed a vincristine resistant and vincristine non-resistant neuroblastoma cell line pair, generated through long-term cultivation of the parental cell line in vincristine or solvent containing medium [40]. Consistent with our hypothesis, the chemotherapy resistant cell model displayed significantly increased ROS-levels, and in turn increased APR-246 sensitivity, when compared to its chemotherapy non-resistant control counterpart (Figure 2d,e).

ROS levels are controlled by intracellular glutathione levels and cysteine importers, such as the cystine-glutamate antiporter encoded by the *SLC7A11* gene. Consequently, low *SLC7A11* expression levels correlate with low amounts of glutathione and high ROS levels. Low amounts of glutathione are completely bound by APR-246/MQ and the expression of *SLC7A11* has been proposed as a predictive biomarker of APR-246 responsiveness in esophagus carcinoma cell lines [19].

To test *SLC7A11* as a response prediction marker for APR-246 sensitivity in pediatric nervous system tumors, we first performed an in silico data analysis of responsive and less-responsive cell lines of the whole Cancer Cell Line Encyclopedia (CCLE), including all cell lines. We divided the cell lines into two groups according to their sensitivity. Based on pharmacokinetics data, we defined the maximum APR-246 trough plasma level of 20 μ M in order to discriminate between responders and low-responders [12]. We then analyzed the *SLC7A11* gene expression in the two CCLE groups [56,57]. Indeed, *SLC7A11* expression was significantly lower in responsive versus low-responsive cell lines (Figure 2f).

In a reverse approach, we investigated which cell lines from which entities displayed low *SLC7A11* expressions. In particular, cell lines of the pediatric entities neuroblastoma and acute lymphoblastic leukemia, as well as adult entities lymphoma and acute myeloid leukemia, expressed *SLC7A11* at a low level. We hypothesized that the low *SLC7A11* expression was associated with a higher responsiveness of these entities to APR-246/PRIMA-1. Combining the expression and sensitivity data confirmed this assumption (Figure 2g, Figure S5). Moreover, *SLC7A11* expression levels of each entity correlated well with their mean APR-246 sensitivity (Pearson correlation coefficient of 0.725) (Figure 2h). Taken together, a low *SLC7A11* expression indicates a high APR-246/PRIMA-1 responsiveness.

Analyzing expression data from the Individualized Therapy For Relapsed Malignancies in Childhood (INFORM) register study using the R2 bioinformatic data analysis platform, we could confirm that neuroblastoma patient samples sensitive to APR-246/PRIMA-1 are characterized by very low *SLC7A11* levels, as compared to most other pediatric enti-

ties. Notably, acute lymphoblastic lymphoma (ALL) and non-Hodgkin lymphoma (NHL) showed a similarly low expression (Figure 2i) [42].

To verify our *in silico* analysis with wet-lab data, we tested seven randomly picked cell line models (four neuroblastoma, two ALL and one non-Hodgkin lymphoma (NHL) cell lines) for APR-246 sensitivity. Six of the seven models were highly responsive to treatment with APR-246 (Table 3).

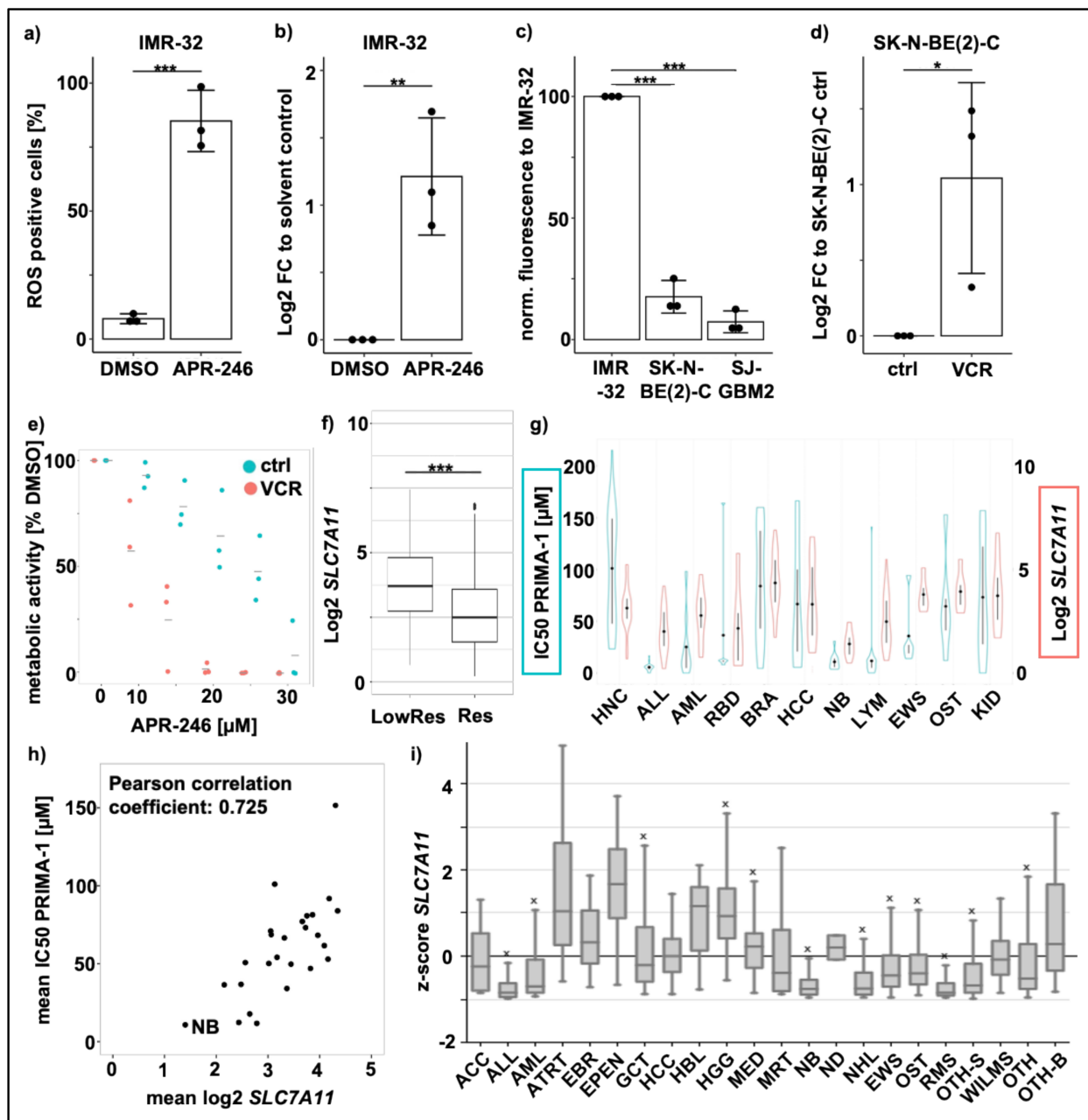


Figure 2. APR-246 response depends on the ROS levels. (a): The percentage of ROS positive IMR-32 cells after treatment with 50 μM APR-246 for 5 h compared to solvent control (DMSO) detected after DCFDA staining by FACS; (b): Log₂ fold change of BODIPY positive IMR-32 cells after treatment with 50 μM APR-246 for 5 h compared to solvent control (DMSO) detected by FACS; (c): Basal ROS level in IMR-32, SK-N-BE(2)-C and SJ-GBM2 detected after DCFDA staining by FACS. Data were normalized to IMR-32 signal; (d): Log₂ fold change of basal ROS level in vincristine resistant SK-N-BE(2)-C compared to control SK-N-BE(2)-C detected after DCFDA staining by FACS; (e): Metabolic activity measurement with CellTiter Glo-assay in vincristine resistant SK-N-BE(2)-C (red) and control SK-N-BE(2)-C (blue) after 72 h treatment with APR-246 0–30 μM . Luminescence was normalized to the respective solvent control (DMSO); (f): Log₂ *SLC7A11* expression of

PRIMA-1 less responsive cell lines (LowRes, IC₅₀ < 20 μM) compared to responsive cell lines (Res, IC₅₀ > 20 μM) from the Cancer Cell Line Encyclopedia ($n = 744$); (g): Combination of log₂ *SLC7A11* expression and PRIMA-1 sensitivity stratified by cancer cell line entities with data obtained from Cancer Cell Line Encyclopedia and CTD² portal ($n = 229$); (h): Plot of the mean log₂ *SLC7A11* expression of entities ($n = 26$) from the CCLE against the mean PRIMA-1 IC₅₀ of the respective entities. Pearson correlation coefficient was calculated using R software; (i) Z-scores of *SLC7A11* log₂ expression from INFORM patient samples stratified by entities and analyzed with R2 ($n = 1643$). ACC: adrenocortical carcinoma, ALL: acute lymphoblastic leukemia, AML: acute myeloid leukemia, ATRT: atypical teratoid/rhabdoid tumor, BRA: Brain cancer, EBR: embryonal brain tumor, EPEN: ependymoma, GCT: germ cell tumor, HCC: hepatocellular carcinoma, HBL: hepatoblastoma, HCC: Liver cancer, HGG: high-grade glioma, HNC: Head and Neck Cancer, KID: Kidney Cancer, LYM: Lymphoma, MED: medulloblastoma, MRT: malignant rhabdoid tumor, NB: neuroblastoma, ND: not defined, NHL: non-Hodgkin lymphoma, EWS: Ewing sarcoma, OST: osteosarcoma, RBD: Rhabdoid, RMS: rhabdomyosarcoma, OTHS: other sarcoma, WILMS: nephroblastoma, OTH: other, OTHB: other brain tumor. * $p < 0.05$, ** $p < 0.01$, *** $p < 0.001$.

Table 3. Sensitivity to APR-246 in seven different models.

Cell Line	Entity	IC ₅₀ /95% CI [μM]	<i>SLC7A11</i> Expression ³
Kelly	Neuroblastoma	8.48/6.8–10.0	1.43
NB-1	Neuroblastoma	4.83/4.22–5.42	1.35
SH-EP	Neuroblastoma	44.5/40.1–49.5	-
SK-N-FI	Neuroblastoma	9.21/8.02–10.1	0.88
NALM-6	ALL ¹	4.56/3.09–6.85	2.51
REH	ALL ¹	4.39/4.0–4.84	1.41
HuT 78	NHL ²	9.47/8.23–10.74	1.45

¹ acute lymphoblastic leukemia. ² non-Hodgkin lymphoma. ³ Log₂ values, derived from CCLE, SH-EP are not included in CCLE.

Taken together our data show that APR-246 treatment results in oxidative stress and cell death and that oxidative stress sensitizes cells to APR-246 treatment. A low *SLC7A11* expression indicates a high APR-246 responsiveness. Entities with rather low *SLC7A11* expression levels (CCLE data) are neuroblastoma, ALL or NHL. A similar *SLC7A11* expression pattern was observed in the INFORM patient cohort, with ALL, rhabdomyosarcoma, NHL and neuroblastoma being those with the lowest *SLC7A11* expressions.

3.3. A Novel Biomarker Signature Improves Response Prediction for Neuroblastoma Cell Lines and Patients

While *SLC7A11* indicates responsiveness quite well for tumor entities, we noticed that the correlation between *SLC7A11* expression and APR-246/PRIMA-1 sensitivity (IC₅₀) was reduced in neuroblastoma cell lines (Pearson correlation coefficient of 0.145, Figure 3a).

To screen for additional novel APR-246/PRIMA-1 response prediction biomarkers in neuroblastoma, we defined two response groups based on the 20 μM plasma trough level threshold: high responders (app. IC₅₀ < 10 μM, 50% plasma trough level) and low-responders (app. IC₅₀ > 40 μM, 200% plasma trough level). We screened R2 gene expression data sets (CCLE) for genes that are differently expressed between high and low-responders (Figure 3b). Among the 171 most significantly differentially expressed genes, 155 genes showed a negative fold change from low-responders to high responders, meaning that these genes were downregulated in responders; 16 genes showing a positive fold change were accordingly upregulated in responders.

The top downregulated gene indicating APR-246 sensitivity was *YAP1* (p -value 1.08×10^{-69} , fold change -2.32 , Figure 3c). The top upregulated gene indicating sensitivity was *MIR142* (p -value 1.28×10^{-58} , fold change 17.75, Figure 3d). We tested the predictive value of the identified genes to classify high-responder/low-responder, resulting in 79.4% (*YAP1*) and 73.5% (*MIR142*) sensitivity and 84.8% (*YAP1*) and 86.1% (*MIR142*) specificity. To generate a biomarker with improved sensitivity and specificity, we combined highly differentially expressed genes to the following gene signature and calculated a

cell lines (PRIMA-1 IC50 app. < 10 μ M, $n = 102$) calculated using R2 software. Except for *YAP1* and *MIR142* (most significantly down and up-regulated gene respectively) all red dots indicate genes that are part of the genetic signature; (c,d): boxplot of z-score of in responsive cell lines that were the most significantly downregulated (c, *YAP1*) and upregulated (d, *MIR142*) genes plotted with R2; (e,f): receiver operating characteristic (ROC) curve calculated with ROCR package in R software for the genetic signature score to discriminate between low-responders (PRIMA-1 IC50 app. > 40 μ M, $n = 303$) and responders (PRIMA-1 IC50 app. < 10 μ M, $n = 102$) (e) or to discriminate the IC50s less than or greater than 20 μ M (f). Responder and low-responder status ($n = 405$) (e) or the whole CCLE cell lines ($n = 711$) with known PRIMA-1 sensitivity data were used as test cohort (f); (g): in silico analysis of genetic signature score predicting PRIMA-1 responsiveness in neuroblastoma sub-cohort from CCLE ($n = 12$). PRIMA-1 sensitivity cut-off 20 μ M was chosen. Ten out of twelve cell lines were predicted correctly. SK-N-SH and SK-N-DZ were falsely predicted to be low-responders. LowRes: low-responder ($n = 303$), Res: responder ($n = 102$).

The optimal cut-off value for a biomarker discriminating between a high responder and low-responder was 1.1, as determined with a receiver operating characteristic (ROC) curve. Higher values indicate higher responsive samples and lower values indicate less responsive samples. The sensitivity at this cut-off was 90.0% and the specificity was 94.3% (Figure 3e). In the next step, we applied the identified gene signature to all cell lines in the CCLE with available sensitivity data and chose the maximum APR-246 plasma trough level of 20 μ M as the sensitivity threshold to be predicted [12]. With this threshold, the most efficient biomarker cut-off was determined to be 1.0, giving a sensitivity of 71.5% and a specificity of 83.8% (Figure 3f). With this biomarker at hand, we again investigated the neuroblastoma sub-cohort of the CCLE and found that 10 out of the 12 models were correctly predicted (Figure 3g).

We further challenged the biomarker's predictions and acquired our own cell culture data from three neuroblastoma models with known expression data, but with unknown sensitivity: SIMA (biomarker 1.80), SH-SY5Y (biomarker 1.68) and SK-N-AS (biomarker 1.03). We expected a cell line with a signature score higher than 1.0 to have an IC50 of below 20 μ M and vice versa. The criteria were met in two of three neuroblastoma cell lines. We also tested three more models of other entities as well as four cultures derived from INFORM patient samples. Notably, the neuroblastoma long-term culture was derived from a neuroblastoma PDX model of an INFORM patient. We identified the APR-246 sensitivity and compared it to the calculated genetic signature score. All three established cell lines (KNS-42, Jurkat, JeKo-1) met the criteria, and three of the four INFORM samples were correctly predicted (Table 4).

Table 4. Biomarker validation in ten randomly picked samples (>1.0 predicts sensitivity; sensitivity is defined as IC50 < 20 μ M).

Model Type	Name/Entity	Biomarker	IC50/95% CI [μ M]
Established cell lines	SK-N-AS/neuroblastoma	1.03	35.1/29.2–43.1
	SIMA/neuroblastoma	1.80	2.04/1.74–2.4
	SH-SY5Y/neuroblastoma	1.68	19.7/16.8–22.4
	KNS-42/pHGG	0.90	27.8/22.8–33.7
	Jurkat/ALL	3.20	1.46/1.38–1.54
	JeKo-1/NHL	5.78	1.44/1.32–1.58
INFORM long-term cultures	INF_R_1288_LTC/rhabdoid tumor	1.09	19.7/14.9–25.8
	INF_R_1467_LTC/soft tissue sarcoma	1.58	18.4/16.9–20.0
INFORM-PDX long-term culture	INF_R_1490_LTC/osteosarcoma	1.19	28.7/25.5–32.0
	INF_R_1632_PDX_LTC/neuroblastoma	3.66	12.2/8.7–16.6

Notably, only 35.5% of all cell lines in the CCLE ($n = 1375$) were predicted to be responders according to our signature score. In contrast, 90.0% of CCLE neuroblastoma cell lines were predicted to be responsive, again highlighting the pronounced sensitivity of this entity to APR-246 treatment.

3.4. Sensitizing Low-Responsive Neuroblastoma Cells to APR-246 Using HDAC-Inhibitors

Despite the generally high responsiveness, our analysis revealed that about 10% of neuroblastoma models were predicted to be less responsive to APR-246. As increased ROS levels augment the effect of APR-246 treatment, we assessed whether we could sensitize low-responsive cells to APR-246 treatment by ROS induction, e.g., by treatment with HDAC inhibitors. HDAC inhibitors are known ROS inducers (reviewed in [59]). We pretreated with 0.5 μM vorinostat for 72 h before addition of 20 μM APR-246 for 24 h and measured cell viability and cell death via trypan blue exclusion assay (Figure 4a–d). Consistent with our hypothesis, both compounds alone showed only minor effects, whereas the combination resulted in a significant reduction in the viable cell number and a significant increase in dead cells in APR-246 low-responsive SK-N-AS and SK-N-BE(2)-C cells.

Similar results were obtained with the HDACi abexinostat, romidepsin and Panobinostat in SK-N-AS, SK-N-BE(2)-C and IMR-32 cells (Table 5). For less responsive SK-N-AS cells at 72 h, co-treatment with HDACi vorinostat resulted in a HSA synergy score of 12.17, which indicated a synergistic effect of the drug combination (Figure 4e,f). In line with our hypothesis, HDACi treatment increased ROS levels in IMR-32 cells and less responsive SK-N-AS cells had a lower basal ROS level compared to responsive IMR-32 cells (Figure S5).

Table 5. HDACi screening for abexinostat, romidepsin and Panobinostat in three neuroblastoma cell line models.

Cell Line	HDAC Inhibitor	IC50 [nM]	95% CI [nM]	+ APR-246 [μM]	IC50 [nM]	95% CI [nM]
SK-N-AS	abexinostat	46.3	29.0–69.8	20	15.4	9.7–23.8
	romidepsin	5.7	4.9–6.6	20	1.8	1.5–2.2
	Panobinostat	2.2	1.6–2.9	20	1.0	0.6–1.4
SK-N-BE(2)-C	abexinostat	172.1	142.2–207.5	10	37.5	22.5–58.9
	romidepsin	26.9	15.2–140.9	10	9.9	3.6–52.9
	Panobinostat	40.2	29.4–54.6	20	3.1	0.3–12.2
IMR-32	abexinostat	100.0	56.3–169.7	2	30.4	6.6–48.9
	romidepsin	0.73	0.64–0.83	1	0.24	0.13–0.33
	Panobinostat	35.6	29.0–43.7	2	13.9	11.0–17.2

To test the combination of the HDAC inhibitor and APR-246 *in vivo*, we used zebrafish embryo neuroblastoma xenograft models of NB-1 and IMR-32 cells. Fluorescently labeled tumor cells were transplanted into the yolk sack on day two post fertilization. Treatment with 50 μM APR-246, 1.5 μM vorinostat, solvent control and the combination was started on day three post fertilization. In both models, decreased tumor growth was observed under treatment with single compounds. However, in both cases the combination was more potent, underlining the effectiveness of combining HDAC inhibition and APR-246 treatment in neuroblastoma models (Figure 4g–n). Taken together, these results demonstrate that combining HDAC inhibition with ROS induction via APR-246 is effective in the treatment of neuroblastoma *in vitro* and *in vivo*.

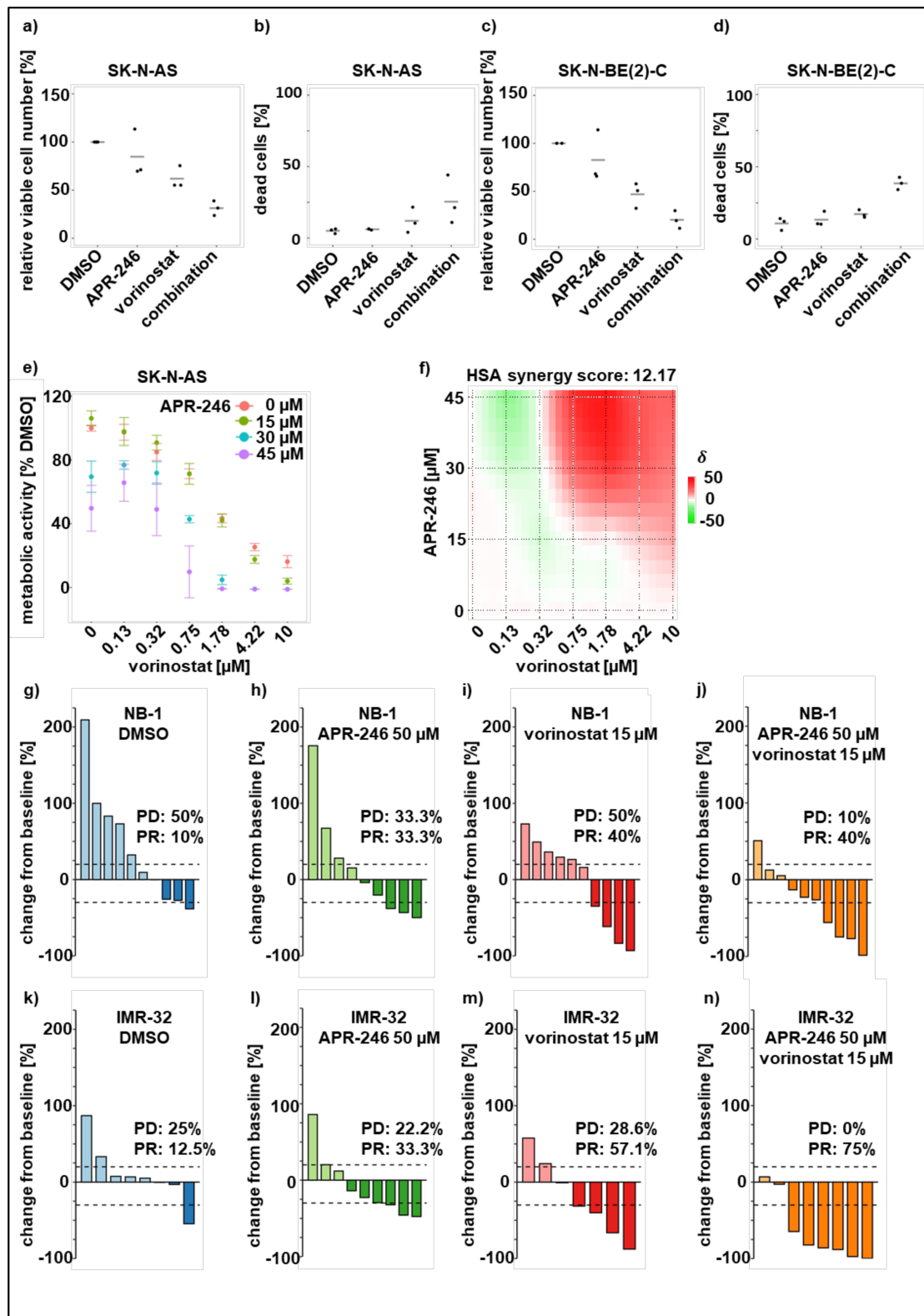


Figure 4. Combining APR-246 with HDAC inhibition effectively sensitizes neuroblastoma in vitro and in vivo. Determination of viable cell number/mL normalized to solvent (DMSO)-treated cells (a,c) and dead cell count (b,d) after automated Trypan blue exclusion assay of neuroblastoma cell lines SK-N-AS and SK-N-BE(2)-C. Cells were pretreated with 0.5 μM vorinostat for 72 h and afterwards treated with 20 μM APR-246 for 24 h. Bars indicate control, single and sequential treatment; (e,f): metabolic activity measurement via CellTiter Glo-assay in neuroblastoma cell line SK-N-AS after 72 h treatment

with 0–10 μM vorinostat combined with fixed APR-246 concentrations of 0 μM , 15 μM , 30 μM and 45 μM . Normalization was performed to the solvent control (DMSO). Synergy calculation (**f**) was performed with synergyfinder (<https://synergyfinder.fimm.fi>, accessed 30 April 2020) by applying HSA (highest single agent) model; (**g–n**): waterfall plots demonstrating the change in tumor volume (%) for each individual xenograft, from baseline (day 1 = start of the treatment) to day 3 after yolk sac-implantation of NB-1 (**g–j**) and IMR-32 (**k–n**) cells. Dotted lines are drawn according to Response Evaluation Criteria in Solid Tumors (RECIST) 1.1 adopted for zebrafish tumors, to visualize the best response: progressive disease (PD), at least a 20% increase in tumor volume; partial response (PR), at least a 30% decrease in tumor volume; each bar reflects one individual xenograft. The following treatments were applied: APR-246: 50 μM ; vorinostat: 15 μM and combination.

4. Discussion

We studied APR-246 as a novel targeted treatment option for pediatric tumors of the nervous system and found neuroblastoma cell lines to be particularly responsive. We established a predictive genetic signature ($\log_2\text{CORO1A} + \log_2\text{RHOH} + \log_2\text{CXCR4} + \log_2\text{PUM2} + \log_2\text{TRAF3IP3} + \log_2\text{KDM2B} + \log_2\text{PDE7A} + \log_2\text{ARHGAP9}$)/($\log_2\text{PLS3} + \log_2\text{RHBDF1} + \log_2\text{CLDN1} + \log_2\text{SLC7A11} + \log_2\text{FAM114A1}$), proposed a novel combinational treatment strategy for neuroblastoma, and validated the cell culture results in the in vivo zebrafish xenotransplantation model. Our results demonstrate that APR-246 is a promising drug candidate for the treatment of neuroblastoma.

The first study to investigate APR-246 in the field of pediatric oncology was conducted using Ewing sarcoma models and was one of the first studies to call p53 reactivation as the main and only mode of action into question [55]. Similar observations were made in a recent study on neuroblastoma. It was stated that APR-246 mainly acts via elevating the ROS level and inhibiting glutathione in this entity. The intracellular amount of glutathione was hypothesized to be modified by MYCN amplification and TP53 mutation status. Notably, the neuroblastoma models used responded extraordinarily well to the treatment [60].

Whereas a relevant number of studies on tumor entities and clinical studies in adults revealed promising effects of APR-246, to our knowledge only a few studies have focused directly on the responsiveness of pediatric entities, including Ewing sarcoma, ALL, diffuse intrinsic pontine glioma, and neuroblastoma [55,60–62]. Recently, the combination of the HDACi Panobinostat and APR-246 has been described to be beneficial in the treatment of glioblastoma cell lines [63]. However, for many entities, the main mode of action of APR-246 remained unclear, predictive biomarkers are needed, and targeted treatment combination partners are missing.

In line with previous reports, we demonstrated that APR-246 responsiveness in pediatric tumors of the nervous system is independent of the TP53 mutation status [60]. We validated a ROS mediated mode of action in neuroblastoma and demonstrated a predictive value of SLC7A11 expression for discriminating responsive from less responsive entities. Using SLC7A11 as a predictive entity marker, we identified ALL and NHL to be very responsive to PRIMA-1/APR-246 treatment. Furthermore, we determined a predictive genetic signature using the CCLE and challenged it with ten randomly picked pediatric cell line models. YAP1 discriminated most significantly between responders and low-responders. YAP1 and the genes from the identified signature may help to identify a novel APR-246 biomarker in other entities in future studies. Interestingly, YAP1 is part of the genetic signature that discriminates between mesenchymal and adrenergic differentiation states in neuroblastoma [64,65]. In line with this, mesenchymal SH-EP and SK-N-AS cells were shown to be less responsive to APR-246, while adrenergic models, such as IMR-32 and SH-SY5Y, were responsive. Whether the neuroblastoma differentiation state is a possible response predictor remains to be further investigated.

Oxidative stress and ROS metabolism have been repeatedly described in the context of drug resistance [66–68]. We consistently found that ROS metabolism is a potential Achilles' heel in acquired drug resistance of neuroblastoma models and highlight the possible use of APR-246 in the targeted treatment of vulnerabilities that are a consequence of chemoresistance. Due to its pharmacokinetics with unusually high plasma concentrations of up to 280 μM and the described mode of action (inhibiting glutathione and thus inducing

ROS) APR-246 constitutes a promising second punch in the one-two punch model. As a first punch, that is supposed to elevate basal ROS levels and thereby increase sensitivity, we applied vorinostat, an HDACi, which was previously described to induce ROS in melanoma [21]. The combination was effective in sensitizing neuroblastoma models and acted synergistically with APR-246. Screening other broad-spectrum HDACis demonstrated that this effect is not vorinostat-exclusive. Identifying the most promising HDACis and investigating selective HDACis to minimize side effects are important future research perspectives.

One restriction of our study is the generally altered ROS metabolism in cell culture models and the question as to how the results can be translated into a clinical context (reviewed in Reference [69]). To address this question, we compared *SLC7A11* expressions in cell lines (CCLE) to *SLC7A11* expressions in patients (INFORM) and found that the same entities express *SLC7A11* low or high in vivo and in vitro. As in vivo metabolism might also alter treatment responses, we tested the HDACi/APR-246 combination in a zebrafish xenograft model and found that it was highly effective. Auspiciously, Wang et al. used a ROS inducing treatment strategy effectively in a patient, highlighting the seminal potential of this approach [21].

Our results and these other preliminary reports underline the possible and promising use of an ROS-inducing treatment strategy for neuroblastoma patients.

5. Conclusions

Our study highlights that ROS induction is a promising novel treatment strategy for neuroblastoma. We established a genetic signature that improves current predictiveness to APR-246 and will help guide future studies. To our knowledge, this is the first report to apply APR-246 and HDACi for the targeted treatment of neuroblastoma. Additionally, we are the first to provide in vivo data for the effective APR-246 treatment of neuroblastoma models.

Supplementary Materials: The following are available online at <https://www.mdpi.com/article/10.3390/cancers13174476/s1>, Figure S1: *TP53* mutation status and PRIMA-1 responsiveness in pediatric entities. Figure S2: APR-246 is not restoring p53 pathway activity in neuroblastoma models IMR-32 (*TP53* wt) and SK-N-BE(2)-C (*TP53*mut, p.C135F). Figure S3: APR-246 is not restoring p53 pathway activity in *TP53* mutant pediatric high-grade glioma models SJ-GBM2 (*TP53*mut p.R273C) and SF188 (*TP53*mut, p.G266E). Figure S4: PRIMA-1 sensitivity and *SLC7A11* expression correlation for Cancer Cell Line Encyclopedia and CTD2 portal cancer entities. Figure S5: SK-N-AS has significantly lower basal ROS level compared to IMR-32 and vorinostat induces ROS in neuroblastoma cell line model.

Author Contributions: Conceptualization, H.P., O.W. and I.O.; methodology, M.M., S.N., C.G., S.K., S.S. and L.R.; software, X.F.G.; validation, M.M., S.N., C.G. and L.R.; formal analysis, M.M., L.R. and X.F.G.; investigation, M.M., J.R., S.N., C.G. and L.R.; resources, J.B., S.K., S.S., F.W., K.F., B.M., T.M., D.T.W.J., O.W. and I.O.; data curation, H.P. and I.O.; writing—original draft preparation, M.M. and I.O.; writing—review and editing, J.R., L.R., J.B., D.T.W.J., K.F., F.W., H.P. and I.O.; visualization, X.F.G.; supervision, H.P., O.W. and I.O.; project administration, O.W. and I.O.; funding acquisition, O.W. and I.O. All authors have read and agreed to the published version of the manuscript.

Funding: This research was funded by German Cancer Aid with Mildred Scheel Doctoral Scholarship, project number 70113124; by SFB 1389-UNITE Glioblastoma, Work Package A02 (OW, DTWJ); the H.W. & J. Hector Foundation, # M91(IO); and Ministry of Rural Affairs and Consumer Protection Baden-Wuerttemberg (IO, ID 4781).

Institutional Review Board Statement: Zebrafish husbandry (permit number 35-9185.64/BH Has-sel/Meder) and experiments (permit number 35-9185.81/G-126/15) were performed according to local animal welfare standards (Tierschutzgesetz §11, Abs. 1, No. 1) and in accordance with European Union animal welfare guidelines (EU Directive 2010/63/EU). All applicable national and institutional guidelines for the care and use of zebrafish were followed. All procedures performed involving animals were in accordance with ethical standards of the institution.

Informed Consent Statement: The INFORM Registry is registered in the German Clinical Trial Register with the following ID: DRKS00007623. Ethics committee approval for INFORM was obtained from Heidelberg University Hospital’s review board. Informed consent was obtained from all subjects involved in the study.

Data Availability Statement: The results published here are fully or partially based upon data generated by the Cancer Target Discovery and Development (CTD²) Network (<https://ocg.cancer.gov/programs/ctd2/data-portal>, accessed on 5 January 2021) established by the National Cancer Institute’s Office of Cancer Genomics. R2 (<http://R2.amc.nl>, accessed on 5 January 2021) and depmap portal (<https://depmap.org/portal/>, accessed on 5 January 2021) were used for in silico analysis. The CCLE datasets are available at the CCLE portal (www.broadinstitute.org/ccle, accessed on 5 January 2021).

Acknowledgments: Graphical Abstract was created with BioRender.com. We thank M. Persicke, T. Grünewald and M. Michaelis for providing cell line models. We thank the inform registry for providing the data used in the cross-entity comparison with primary cancer/leukemia samples. Support from the DKFZ Core Facility Tumor Models (Karin Müller-Decker) is gratefully acknowledged. Moreover, we thank Alexandra Stroh-Dege, Young-Gyu Park and Aileen Mangan for excellent technical assistance.

Conflicts of Interest: The authors declare no conflict of interest.

References

1. Brodeur, G.M. Neuroblastoma: Biological insights into a clinical enigma. *Nat. Rev. Cancer* **2003**, *3*, 203–216. [[CrossRef](#)] [[PubMed](#)]
2. Cohn, S.L.; Pearson, A.D.; London, W.B.; Monclair, T.; Ambros, P.F.; Brodeur, G.M.; Faldum, A.; Hero, B.; Iehara, T.; Machin, D.; et al. The International Neuroblastoma Risk Group (INRG) classification system: An INRG task force report. *J. Clin. Oncol.* **2009**, *27*, 289–297. [[CrossRef](#)]
3. Monclair, T.; Brodeur, G.M.; Ambros, P.F.; Brisse, H.J.; Cecchetto, G.; Holmes, K.; Kaneko, M.; London, W.B.; Matthay, K.K.; Nuchtern, J.G.; et al. The International Neuroblastoma Risk Group (INRG) staging system: An INRG task force report. *J. Clin. Oncol.* **2009**, *27*, 298–303. [[CrossRef](#)]
4. Neuroblastoma Treatment (PDQ®)—Health Professional Version. Available online: https://www.cancer.gov/types/neuroblastoma/hp/neuroblastoma-treatment-pdq#_534_toc (accessed on 1 February 2021).
5. Wasylshen, A.R.; Lozano, G. Attenuating the p53 pathway in human cancers: Many means to the same end. *Cold Spring Harb Perspect. Med.* **2016**, *6*, a026211. [[CrossRef](#)]
6. Ackermann, S.; Cartolano, M.; Hero, B.; Welte, A.; Kahlert, Y.; Roderwieser, A.; Bartenhagen, C.; Walter, E.; Gecht, J.; Kerschke, L.; et al. A mechanistic classification of clinical phenotypes in neuroblastoma. *Science* **2018**, *362*, 1165–1170. [[CrossRef](#)] [[PubMed](#)]
7. Tweddle, D.A.; Malcolm, A.J.; Cole, M.; Pearson, A.D.; Lunec, J. p53 cellular localization and function in neuroblastoma: Evidence for defective G(1) arrest despite WAF1 induction in MYCN-amplified cells. *Am. J. Pathol.* **2001**, *158*, 2067–2077. [[CrossRef](#)]
8. Isaacs, J.S.; Hardman, R.; Carman, T.A.; Barrett, J.C.; Weissman, B.E. Differential subcellular p53 localization and function in N- and S-type neuroblastoma cell lines. *Cell Growth Differ.* **1998**, *9*, 545–555. [[PubMed](#)]
9. Moll, U.M.; LaQuaglia, M.; Bénard, J.; Riou, G. Wild-type p53 protein undergoes cytoplasmic sequestration in undifferentiated neuroblastomas but not in differentiated tumors. *Proc. Natl. Acad. Sci. USA* **1995**, *92*, 4407–4411. [[CrossRef](#)] [[PubMed](#)]
10. Duffy, M.J.; Synnott, N.C.; Crown, J. Mutant p53 as a target for cancer treatment. *Eur. J. Cancer* **2017**, *83*, 258–265. [[CrossRef](#)]
11. Aprea Therapeutics Website: Our Clinical Trials. Available online: <https://www.aprea.com/clinical-trials/> (accessed on 1 February 2021).
12. Lehmann, S.; Bykov, V.J.; Ali, D.; Andrén, O.; Cherif, H.; Tidefelt, U.; Uggla, B.; Yachnin, J.; Juliusson, G.; Moshfegh, A.; et al. Targeting p53 in vivo: A first-in-human study with p53-targeting compound APR-246 in refractory hematologic malignancies and prostate cancer. *J. Clin. Oncol.* **2012**, *30*, 3633–3639. [[CrossRef](#)] [[PubMed](#)]
13. Deneberg, S.; Cherif, H.; Lazarevic, V.; Andersson, P.O.; von Euler, M.; Juliusson, G.; Lehmann, S. An open-label phase I dose-finding study of APR-246 in hematological malignancies. *Blood Cancer J.* **2016**, *6*, e447. [[CrossRef](#)]
14. Bykov, V.J.; Zache, N.; Stridh, H.; Westman, J.; Bergman, J.; Selivanova, G.; Wiman, K.G. PRIMA-1(MET) synergizes with cisplatin to induce tumor cell apoptosis. *Oncogene* **2005**, *24*, 3484–3491. [[CrossRef](#)]
15. Bykov, V.J.; Issaeva, N.; Shilov, A.; Hultcrantz, M.; Pugacheva, E.; Chumakov, P.; Bergman, J.; Wiman, K.G.; Selivanova, G. Restoration of the tumor suppressor function to mutant p53 by a low-molecular-weight compound. *Nat. Med.* **2002**, *8*, 282–288. [[CrossRef](#)]
16. Lambert, J.M.; Gorzov, P.; Veprintsev, D.B.; Söderqvist, M.; Segerbäck, D.; Bergman, J.; Fersht, A.R.; Hainaut, P.; Wiman, K.G.; Bykov, V.J. PRIMA-1 reactivates mutant p53 by covalent binding to the core domain. *Cancer Cell* **2009**, *15*, 376–388. [[CrossRef](#)]
17. Zhang, Q.; Bykov, V.J.N.; Wiman, K.G.; Zawacka-Pankau, J. APR-246 reactivates mutant p53 by targeting cysteines 124 and 277. *Cell Death Dis.* **2018**, *9*, 439. [[CrossRef](#)] [[PubMed](#)]

18. Peng, X.; Zhang, M.Q.Z.; Conserva, F.; Hosny, G.; Selivanova, G.; Bykov, V.J.N.; Arnér, E.S.J.; Wiman, K.G. APR-246/PRIMA-1MET inhibits thioredoxin reductase 1 and converts the enzyme to a dedicated NADPH oxidase. *Cell Death Dis.* **2013**, *4*, e881. [[CrossRef](#)]
19. Liu, D.S.; Duong, C.P.; Haupt, S.; Montgomery, K.G.; House, C.M.; Azar, W.J.; Pearson, H.B.; Fisher, O.M.; Read, M.; Guerra, G.R.; et al. Inhibiting the system x(C)(-)/glutathione axis selectively targets cancers with mutant-p53 accumulation. *Nat. Commun.* **2017**, *8*, 14844. [[CrossRef](#)] [[PubMed](#)]
20. Storz, P. Reactive oxygen species in tumor progression. *Front. Biosci.* **2005**, *10*, 1881–1896. [[CrossRef](#)] [[PubMed](#)]
21. Wang, L.; Leite de Oliveira, R.; Huijberts, S.; Bosdriesz, E.; Pencheva, N.; Brunen, D.; Bosma, A.; Song, J.Y.; Zevenhoven, J.; Los-de Vries, G.T.; et al. An acquired vulnerability of drug-resistant melanoma with therapeutic potential. *Cell* **2018**, *173*, 1413–1425. [[CrossRef](#)]
22. Koeneke, E.; Witt, O.; Oehme, I. HDAC family members intertwined in the regulation of autophagy: A druggable vulnerability in aggressive tumor entities. *Cells* **2015**, *4*, 135–168. [[CrossRef](#)]
23. Ridinger, J.; Koeneke, E.; Kolbinger, F.R.; Koerholz, K.; Mahboobi, S.; Hellweg, L.; Gunkel, N.; Miller, A.K.; Peterziel, H.; Schmezer, P.; et al. Dual role of HDAC10 in lysosomal exocytosis and DNA repair promotes neuroblastoma chemoresistance. *Sci. Rep.* **2018**, *8*, 10039. [[CrossRef](#)]
24. Fabian, J.; Lodrini, M.; Oehme, I.; Schier, M.C.; Thole, T.M.; Hielscher, T.; Kopp-Schneider, A.; Opitz, L.; Capper, D.; von Deimling, A.; et al. GRHL1 acts as tumor suppressor in neuroblastoma and is negatively regulated by MYCN and HDAC3. *Cancer Res.* **2014**, *74*, 2604–2616. [[CrossRef](#)] [[PubMed](#)]
25. Ecker, J.; Oehme, I.; Mazitschek, R.; Korshunov, A.; Kool, M.; Hielscher, T.; Kiss, J.; Selt, F.; Konrad, C.; Lodrini, M.; et al. Targeting class I histone deacetylase 2 in MYC amplified group 3 medulloblastoma. *Acta Neuropathol. Commun.* **2015**, *3*, 22. [[CrossRef](#)] [[PubMed](#)]
26. Oehme, I.; Lodrini, M.; Brady, N.R.; Witt, O. Histone deacetylase 10-promoted autophagy as a druggable point of interference to improve the treatment response of advanced neuroblastomas. *Autophagy* **2013**, *9*, 2163–2165. [[CrossRef](#)] [[PubMed](#)]
27. Oehme, I.; Linke, J.P.; Bock, B.C.; Milde, T.; Lodrini, M.; Hartenstein, B.; Wiegand, I.; Eckert, C.; Roth, W.; Kool, M.; et al. Histone deacetylase 10 promotes autophagy-mediated cell survival. *Proc. Natl. Acad. Sci. USA* **2013**, *110*, E2592–E2601. [[CrossRef](#)] [[PubMed](#)]
28. Oehme, I.; Deubzer, H.E.; Wegener, D.; Pickert, D.; Linke, J.P.; Hero, B.; Kopp-Schneider, A.; Westermann, F.; Ulrich, S.M.; von Deimling, A.; et al. Histone deacetylase 8 in neuroblastoma tumorigenesis. *Clin. Cancer Res.* **2009**, *15*, 91–99. [[CrossRef](#)]
29. Witt, O.; Deubzer, H.E.; Lodrini, M.; Milde, T.; Oehme, I. Targeting histone deacetylases in neuroblastoma. *Curr. Pharm. Des.* **2009**, *15*, 436–447. [[CrossRef](#)]
30. Kolbinger, F.R.; Koeneke, E.; Ridinger, J.; Heimburg, T.; Muller, M.; Bayer, T.; Sippl, W.; Jung, M.; Gunkel, N.; Miller, A.K.; et al. The HDAC6/8/10 inhibitor TH34 induces DNA damage-mediated cell death in human high-grade neuroblastoma cell lines. *Arch. Toxicol.* **2018**, *92*, 2649–2664. [[CrossRef](#)] [[PubMed](#)]
31. Milde, T.; Oehme, I.; Korshunov, A.; Kopp-Schneider, A.; Remke, M.; Northcott, P.; Deubzer, H.E.; Lodrini, M.; Taylor, M.D.; von Deimling, A.; et al. HDAC5 and HDAC9 in medulloblastoma: Novel markers for risk stratification and role in tumor cell growth. *Clin. Cancer Res.* **2010**, *16*, 3240–3252. [[CrossRef](#)]
32. El-Naggar, A.M.; Somasekharan, S.P.; Wang, Y.; Cheng, H.; Negri, G.L.; Pan, M.; Wang, X.Q.; Delaidelli, A.; Rafn, B.; Cran, J.; et al. Class I HDAC inhibitors enhance YB-1 acetylation and oxidative stress to block sarcoma metastasis. *EMBO Rep.* **2019**, *20*, e48375. [[CrossRef](#)]
33. Anastas, J.N.; Zee, B.M.; Kalin, J.H.; Kim, M.; Guo, R.; Alexandrescu, S.; Blanco, M.A.; Giera, S.; Gillespie, S.M.; Das, J.; et al. Re-programming Chromatin with a Bifunctional LSD1/HDAC Inhibitor Induces Therapeutic Differentiation in DIPG. *Cancer Cell* **2019**, *36*, e510. [[CrossRef](#)]
34. West, A.C.; Johnstone, R.W. New and emerging HDAC inhibitors for cancer treatment. *J. Clin. Investig.* **2014**, *124*, 30–39. [[CrossRef](#)] [[PubMed](#)]
35. Falkenberg, K.J.; Johnstone, R.W. Histone deacetylases and their inhibitors in cancer, neurological diseases and immune disorders. *Nat. Rev. Drug Discov.* **2014**, *13*, 673–691. [[CrossRef](#)]
36. Witt, O.; Milde, T.; Deubzer, H.E.; Oehme, I.; Witt, R.; Kulozik, A.; Eisenmenger, A.; Abel, U.; Karapanagiotou-Schenkel, I. Phase I/II intra-patient dose escalation study of vorinostat in children with relapsed solid tumor, lymphoma or leukemia. *Klin. Padiatr.* **2012**, *224*, 398–403. [[CrossRef](#)]
37. National Center for Biotechnology Information. PubChem Compound Summary for CID 322968, Prima-1. Available online: <https://pubchem.ncbi.nlm.nih.gov/compound/Prima-1> (accessed on 8 May 2021).
38. National Center for Biotechnology Information. PubChem Compound Summary for CID 52918385, Prima-1met. Available online: <https://pubchem.ncbi.nlm.nih.gov/compound/Prima-1met> (accessed on 8 May 2021).
39. National Center for Biotechnology Information. PubChem Compound Summary for CID 322973, 2-Methylenequinuclidin-3-one. Available online: <https://pubchem.ncbi.nlm.nih.gov/compound/2-Methylenequinuclidin-3-one> (accessed on 8 May 2021).
40. Jemaà, M.; Sime, W.; Abassi, Y.; Lasorsa, V.A.; Bonne Køhler, J.; Michaelis, M.; Cinatl, J., Jr.; Capasso, M.; Massoumi, R. Gene expression signature of acquired chemoresistance in neuroblastoma cells. *Int. J. Mol. Sci.* **2020**, *21*, 5811. [[CrossRef](#)] [[PubMed](#)]
41. Sapio, R.T.; Nezydur, A.N.; Krevetski, M.; Anikin, L.; Manna, V.J.; Minkovsky, N.; Pestov, D.G. Inhibition of post-transcriptional steps in ribosome biogenesis confers cytoprotection against chemotherapeutic agents in a p53-dependent manner. *Sci. Rep.* **2017**, *7*, 9041. [[CrossRef](#)] [[PubMed](#)]

42. Worst, B.C.; van Tilburg, C.M.; Balasubramanian, G.P.; Fiesel, P.; Witt, R.; Freitag, A.; Boudalil, M.; Previti, C.; Wolf, S.; Schmidt, S.; et al. Next-generation personalized medicine for high-risk pediatric cancer patients—The INFORM pilot study. *Eur. J. Cancer* **2016**, *65*, 91–101. [CrossRef]
43. Lin, G.L.; Monje, M. A protocol for rapid post-mortem cell culture of Diffuse Intrinsic Pontine Glioma (DIPG). *J. Vis. Exp.* **2017**, *9*, 5233–5250. [CrossRef] [PubMed]
44. Stewart, E.; Federico, S.M.; Chen, X.; Shelat, A.A.; Bradley, C.; Gordon, B.; Karlstrom, A.; Twarog, N.R.; Clay, M.R.; Bahrami, A.; et al. Orthotopic patient-derived xenografts of pediatric solid tumors. *Nature* **2017**, *549*, 96–100. [CrossRef]
45. Fischer, M.; Skowron, M.; Berthold, F. Reliable transcript quantification by real-time reverse transcriptase-polymerase chain reaction in primary neuroblastoma using normalization to averaged expression levels of the control genes HPRT1 and SDHA. *J. Mol. Diagn.* **2005**, *7*, 89–96. [CrossRef]
46. Witt, O.; Monkemeyer, S.; Ronndahl, G.; Erdlenbruch, B.; Reinhardt, D.; Kanbach, K.; Pekrun, A. Induction of fetal hemoglobin expression by the histone deacetylase inhibitor apicidin. *Blood* **2003**, *101*, 2001–2007. [CrossRef]
47. Livak, K.J.; Schmittgen, T.D. Analysis of relative gene expression data using real-time quantitative PCR and the 2(-Delta Delta C(T)) Method. *Methods* **2001**, *25*, 402–408. [CrossRef] [PubMed]
48. Wrobel, J.K.; Najafi, S.; Ayhan, S.; Gatzweiler, C.; Kronic, D.; Ridinger, J.; Milde, T.; Westermann, F.; Peterziel, H.; Meder, B.; et al. Rapid in vivo validation of HDAC inhibitor-based treatments in neuroblastoma zebrafish xenografts. *Pharmaceuticals* **2020**, *13*, 345. [CrossRef]
49. Aksoy, B.A.; Dancik, V.; Smith, K.; Mazerik, J.N.; Ji, Z.; Gross, B.; Nikolova, O.; Jaber, N.; Califano, A.; Schreiber, S.L.; et al. CTD2 Dashboard: A searchable web interface to connect validated results from the Cancer Target Discovery and Development Network. *Database* **2017**, *11*, 7400. [CrossRef]
50. Rees, M.G.; Seashore-Ludlow, B.; Cheah, J.H.; Adams, D.J.; Price, E.V.; Gill, S.; Javaid, S.; Coletti, M.E.; Jones, V.L.; Bodycombe, N.E.; et al. Correlating chemical sensitivity and basal gene expression reveals mechanism of action. *Nat. Chem. Biol.* **2016**, *12*, 109–116. [CrossRef] [PubMed]
51. Seashore-Ludlow, B.; Rees, M.G.; Cheah, J.H.; Cokol, M.; Price, E.V.; Coletti, M.E.; Jones, V.; Bodycombe, N.E.; Soule, C.K.; Gould, J.; et al. Harnessing Connectivity in a Large-Scale Small-Molecule Sensitivity Dataset. *Cancer Discov.* **2015**, *5*, 1210–1223. [CrossRef] [PubMed]
52. Basu, A.; Bodycombe, N.E.; Cheah, J.H.; Price, E.V.; Liu, K.; Schaefer, G.I.; Ebright, R.Y.; Stewart, M.L.; Ito, D.; Wang, S.; et al. An interactive resource to identify cancer genetic and lineage dependencies targeted by small molecules. *Cell* **2013**, *154*, 1151–1161. [CrossRef] [PubMed]
53. Ianevski, A.; Giri, A.K.; Aittokallio, T. SynergyFinder 2.0: Visual analytics of multi-drug combination synergies. *Nucleic Acids Res.* **2020**, *48*, W488–W493. [CrossRef] [PubMed]
54. Lu, T.; Zou, Y.; Xu, G.; Potter, J.A.; Taylor, G.L.; Duan, Q.; Yang, Q.; Xiong, H.; Qiu, H.; Ye, D.; et al. PRIMA-1Met suppresses colorectal cancer independent of p53 by targeting MEK. *Oncotarget* **2016**, *7*, 83017–83030. [CrossRef]
55. Aryee, D.N.T.; Niedan, S.; Ban, J.; Schwentner, R.; Muehlbacher, K.; Kauer, M.; Kofler, R.; Kovar, H. Variability in functional p53 reactivation by PRIMA-1Met/APR-246 in Ewing sarcoma. *Br. J. Cancer* **2013**, *109*, 2696–2704. [CrossRef] [PubMed]
56. Depmap Release: Broad, D. Public_21q1. 2021. Available online: <https://doi.org/10.6084/m9.figshare.13681534.v1> (accessed on 5 January 2021). [CrossRef]
57. Barretina, J.; Caponigro, G.; Stransky, N.; Venkatesan, K.; Margolin, A.A.; Kim, S.; Wilson, C.J.; Lehár, J.; Kryukov, G.V.; Sonkin, D.; et al. The Cancer Cell Line Encyclopedia enables predictive modelling of anticancer drug sensitivity. *Nature* **2012**, *483*, 603–607. [CrossRef]
58. Kato, S.; Han, S.-Y.; Liu, W.; Otsuka, K.; Shibata, H.; Kanamaru, R.; Ishioka, C. Understanding the function–structure and function–mutation relationships of p53 tumor suppressor protein by high-resolution missense mutation analysis. *Proc. Natl. Acad. Sci. USA* **2003**, *100*, 8424. [CrossRef] [PubMed]
59. Sultana, F.; Manasa, K.L.; Shaik, S.P.; Bonam, S.R.; Kamal, A. Zinc dependent histone deacetylase inhibitors in cancer therapeutics: Recent update. *Curr. Med. Chem.* **2019**, *26*, 7212–7280. [CrossRef] [PubMed]
60. Mlakar, V.; Jurkovic Mlakar, S.; Lesne, L.; Marino, D.; Rathi, K.S.; Maris, J.M.; Ansari, M.; Gummy-Pause, F. PRIMA-1(MET)-induced neuroblastoma cell death is modulated by p53 and mycn through glutathione level. *J. Exp. Clin. Cancer Res.* **2019**, *38*, 69. [CrossRef] [PubMed]
61. Demir, S.; Boldrin, E.; Sun, Q.; Hampp, S.; Tausch, E.; Eckert, C.; Ebinger, M.; Handgretinger, R.; Kronnie, G.T.; Wiesmüller, L.; et al. Therapeutic targeting of mutant p53 in pediatric acute lymphoblastic leukemia. *Haematologica* **2020**, *105*, 170–181. [CrossRef] [PubMed]
62. Nikolaev, A.; Fiveash, J.B.; Yang, E.S. Combined targeting of mutant p53 and Jumonji family histone demethylase augments therapeutic efficacy of radiation in H3K27M DIPG. *Int. J. Mol. Sci.* **2020**, *21*, 490. [CrossRef] [PubMed]
63. De La Rosa, J.; Urdiciain, A.; Zelaya, M.V.; Zazpe, I.; Meléndez, B.; Rey, J.A.; Idoate, M.A.; Castresana, J.S. APR-246 combined with 3-deazaneplanocin A, panobinostat or temozolomide reduces clonogenicity and induces apoptosis in glioblastoma cells. *Int. J. Oncol.* **2021**, *58*, 312–330. [CrossRef]
64. van Groningen, T.; Akogul, N.; Westerhout, E.M.; Chan, A.; Hasselt, N.E.; Zwijnenburg, D.A.; Broekmans, M.; Stroeken, P.; Haneveld, F.; Hooijer, G.K.J.; et al. A NOTCH feed-forward loop drives reprogramming from adrenergic to mesenchymal state in neuroblastoma. *Nat. Commun.* **2019**, *10*, 1530. [CrossRef] [PubMed]

-
65. Groningen, T.; Koster, J.; Valentijn, L.; Zwijnenburg, D.; Akogul, N.; Hasselt, N.; Broekmans, M.; Haneveld, F.; Nowakowska, N.; Bras, J.; et al. Neuroblastoma is composed of two super-enhancer-associated differentiation states. *Nat. Genet.* **2017**, *49*, 1261–1266. [[CrossRef](#)]
 66. Cen, J.; Zhang, L.; Liu, F.; Zhang, F.; Ji, B.S. Long-term alteration of reactive oxygen species led to multidrug resistance in MCF-7 cells. *Oxid Med. Cell Longev.* **2016**, *2016*, 7053451. [[CrossRef](#)]
 67. Waghela, B.N.; Vaidya, F.U.; Pathak, C. Upregulation of NOX-2 and Nrf-2 promotes 5-Fluorouracil resistance of human colon carcinoma (HCT-116) cells. *Biochemistry* **2021**, *86*, 262–274. [[CrossRef](#)] [[PubMed](#)]
 68. Zhao, X.; Quan, J.; Tan, Y.; Liu, Y.; Liao, C.; Li, Z.; Liao, W.; Liu, J.; Cao, Y.; Luo, X. RIP3 mediates TCN-induced necroptosis through activating mitochondrial metabolism and ROS production in chemotherapy-resistant cancers. *Am. J. Cancer Res.* **2021**, *11*, 729–745. [[PubMed](#)]
 69. Halliwell, B. Cell culture, oxidative stress, and antioxidants: Avoiding pitfalls. *Biomed. J.* **2014**, *37*, 99–105. [[CrossRef](#)] [[PubMed](#)]